MuID Square-Hole Shielding Study.

February 22sd 2002

Vince Cianciolo, Andrew Glenn, George Gogiberizde, Jason Newby, Kenneth Read, Hiroki Sato, Soren Sorensen, Atsushi Taketani, Laurence Villatte

Studying the rejection factor for the level 2 trigger of the muon arm, using simulated Au-Au collisions, it was observed that a large number of particles making a hit in the Muon Identifier (MuID), were produced in the beam-pipe. At the same time, the comparison of the number of hits per gap extracted from the simulation and the experimental data showed that the simulated hits were underestimated by a factor 2.-2.5 (after adding the DX magnet in PISA simulation).

After obtaining the first value of the rejection factor for the real data, it was decided to add shielding in the square-hole of the MuID in order to eliminate the particles coming from the beam-pipe and the DX magnet. To determine the most appropriate shielding, we first had to improve the simulation in order that it reproduced as well as possible the real data with different configurations of shielding.

1 Preliminary tests.

1.1 Hit rate versus BBC charge.

Before investigating an improvement of the simulations it was tested that the extra hits observed in the real data do not come from beam-gas interaction. To check this, we looked at the spectrum of the number of hits in the MuID versus the charge collected in the BBC detectors as illustrated in figure 1. On this figure, we observe that the hit rate in the MuID and the BBC charge are strongly correlated. If the extra hits corresponded to beam-gas interactions, one should expect many hits in peripheral events or a broad distribution if it was due to accidentals.

1.2 Timing of the detector.

Figures 2 and 3 present the distribution of the time delay (in beam clock unit) for an event to be accepted by the Beam-Beam Local Level 1 trigger obtained for the cables corresponding to the horizontal (figure 2) and vertical (figure 3) tubes in gap 0 (chosen as an example) of the MuID. On these plots, we observe for each cable a narrow peak of mean value 10 beam clock units. These distributions correspond to Minimum Bias events triggered on the BBC, so the hits at the peak come primarily from real events. The fact that we do not see hits outside the peak shows that we do not see many hits uncorrelated with a real interaction.

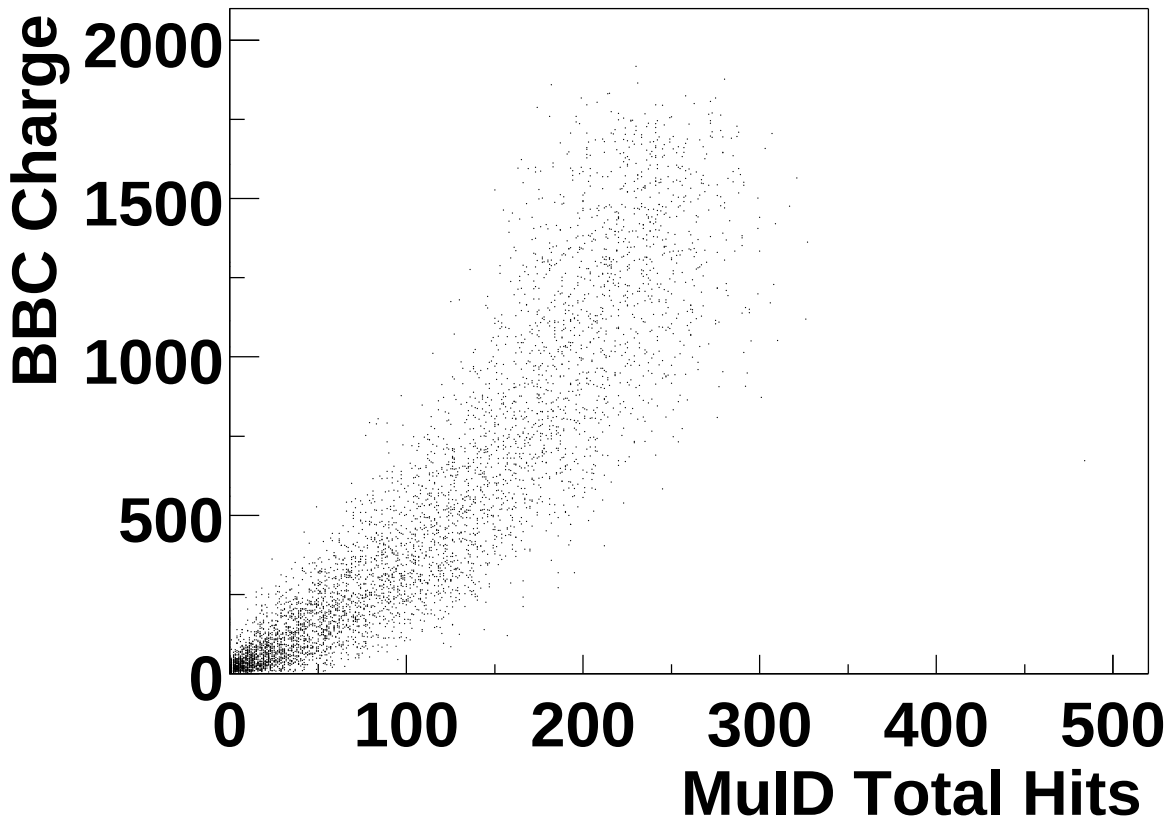

Figure 1: *Hit rate in the MuID versus the charge collected in the BBC detectors.*

2 Improvement of the simulation.

As said previously, with the number of simulated hits in the MuID obtained from the original simulation, using HIJING generator, being 60% lower than the number observed from the real data, it was decided to improve the simulation in order that it reproduced as well as possible the experimental occupancy.

Figure 4 presents the number of hits per event (summed over the panels) as a function of gap extracted from the real data (black squares) and the previous simulation noted "old"(stars). Here we observe the average factor of about 2-2.5 between the simulation and the real data.

The main improvement to the simulation consists of 3 important changes:

- to consider the 3D momentum of the particles to determine the PISA hit locations in the MuID (whereas before all the particles were taken with a momentum parallel to the beam axis)
- to allow multiple hits for one particle in different tubes in the same gap
- to increase the sensitive volume which determines the struck tubes

The simulation was fine for the particles entering parallel or close to parallel to the beam

axis, as has been expected. These changes were essentially important to improve the efficiency for the particles entering the panels transversly (to the beam axis).

The result of this improvement is shown in figure 4 by the circles, marked "new response chain".

An additional improvement was done by decreasing the photon threshold in the absorbers of the MuID (in the inner absorber part, the threshold was put to 5 MeV instead of 50 MeV). The results of this simulation, using also the new response chain, is represented by the triangles in figure 4. So, reducing the photon threshold in the MuID absorbers increases the hit occupancy of a further 10%.

3 Origin of the particles hitting the MuID.

Creation point of the particles which fire the Iarocci tubes.

Although not previously recognized, even according to the original simulations a large fraction of the particles which produce a hit in the MuID are produced in the beam-pipe and the DX magnet. This is illustrated by figure 5 which shows the radial coordinate versus the z value along the beam axis of the creation point of the particles which have generated a hit in the MuID. As previously [1], on figure 5 we observe different structures corresponding to elements of the experimental setup and of the collider (these elements are indicated in figure 5).

Primary particles generating a hit in the MuID.

To go farther in the study of the origin of the particles firing the MuID, we followed their ancestry to the PISA input. Figure 6 shows the pseudo-rapidity distribution per event of the primaries (after the improvement of the simulation) which cause a hit in the MuID for 3 different impact parameter selections. The nominal pseudo-rapidity acceptance of the MuID ([-2.4,-1.2]) and the pseudo-rapidity corresponding to the beam-pipe in the z-range of the square-hole of the MuID ([-5.65,-5.4]) are indicated. We note that only a small fraction of the particles producing a hit in the MuID come from the MuID acceptance. On the contrary, we observe a peak corresponding to primaries hitting the beam-pipe in the square-hole. Then, either particles produced in the beam-pipe (or the DX magnet) or their daughters created in the MuID sensitive volume fire the Iarocci tubes.

Hence, according to the simulations approximately 80 % of the hits come from primaries hitting material inside the square-hole. Even before improving the simulation, the primary particles were dominated by a peak corresponding to $\eta < -5$. But as these particles necessarily enter mainly the MuID transversely to the beam axis, the previous response chain was inefficient for a large part of them, which explains why the simulation was in disagreement with the real data.

The x-y distributions of the hits in gap 0 corresponding to primaries with $y_{prim} > -3$ (roughly in MuID accepatence) and $y_{prim} < -3$ are shown in figures 7 and 8. (*Note:* although we use gap 0 as an example, we see the same effects in the other gaps) . We observe that the hits coming from primaries with $y_{prim} > -3$ are relatively evenly distributed whereas for $y_{prim} < -3$ we observe a very large occupancy in the center around the square-hole which is very similar to what is observed for the experimental occupancy. This exhibits again the fact that in the real data there is a lot of hits which originate in the beam-pipe and the square-hole, and that we do not want to record.

HIJING checking.

As the simulation points out that a large number of primary particles interact in the beam-pipe (corresponding to $\eta = [-5.65, -5.4]$), we wanted to check that the charged particle multiplicity in the pseudo-rapidity region $-5.65 \leq \eta \leq -5.4$ obtained from HIJING is correct. Charged multiplicity yields from RHIC at these large η values do not exist. However, in reference [2] it was shown that the charged multiplicity in the projectile region in AB collisions at CERN/SPS is well described by a combination of limiting fragmentation and the wounded nucleon model, see figure 9. The hypothesis of limiting fragmentation states that in pp and $\bar{p}p$ collisions the multiplicity in the projectile region is independent of the beam energy. According to the wounded nucleon model the mulplicity of the particles produced in soft collisions is proportional to the number of participant nucleons in the collision N_{part}. Since all the particles near the projectile rapidity are necessarily produced by soft collisions, combining these hypothesizes states that the particle production, scaled by N_{part}, is independant of the projectile size. Figure 9 from [2] presents the charged density divided by N_{part}^{beam}, the number of participant nucleons from the beam nucleus, in the beam frame $\eta' = |\eta| - |y^{beam}|$ where y^{beam} is the rapidity of the beam. BRAHMS experiment [3] verified that scaling at RHIC energy $\sqrt{s} = 130$ GeV for $-2 < \eta' < -0.3$, as shown in figure 10 (inserted spectrum), so we feel safe extrapolating to $0.04 < \eta' < 0.29$: $(dN/d\eta')/(N_{part}/2) \approx 0.4$, so $\Delta N(0.04 \leq \eta' \leq 0.29) = 0.05 \times N_{part}$.

The charged particle multiplicity for $0.04 \leq \eta' \leq 0.29$ versus N_{part} extracted from HIJING is shown in figure 11 as well as the charged multiplicity dependance deduced from the hypothesis of limiting fragmentation. From figure 11, we conclude that the charged multiplicity in $\eta' = [0.04, 0.29]$ obtained from HIJING is in rough agreement with the predicted value.

4 Shielding study.

Momentum spectra.

To estimate what would be the best shielding, we first looked at the momentum distribution of the particles for which a hit has been recorded in the MuID and which was created in the beam-pipe region or the DX magnet region. Figure 12 presents the momentum distribution of the electrons, positrons, pions and protons (the main particles which originate hits) when they enter the sensitive volume (i.e. the MuID). On figure 12 is also indicated the upper limit of the momentum range corresponding to the particles stopped by different thicknesses and materials. *Note:* the momentum was low enough that the stopping power was material-independent and the figure of merit was the total weight of material or equivalently the area density (g/cm^2).

We can see that one inch of aluminium should eliminate 75 % of the electrons and positrons but it would only reduce by approximately 5 % the numbers of pions and by 41 % the number of protons hitting the MuID. The difference between 3" and 6" of iron is mainly important for reducing the fraction of pions created in the square hole region that can produce a hit in the MuID: from 67 % to 36 %. The background could be further reduced by putting even more shielding, but 6" of iron pushed the limit of practicality for this year's run.

Tests with real data.

To determine the best configuration of the shielding (thickness, geometry...), we did tests with real data using different kinds of shielding installed in gap 4 (last gap) and gap 3, as described below:

- "None": no added shielding (i.e. only the Aluminium floor, 0.5" of Al)
- "Aluminium": 1" of Al in the bottom of gap 4 + 1" of Al in the sides of gap 4 (+ Aluminium floor)
- "2" iron": 2" of iron in the bottom of gap 4 and gap 3 + 1" of Al in the sides of gap 4 + 1" of Al in the sides of gap 4 (+ Aluminium floor)
- "6" iron": 6" of iron in the bottom of gap 4 + 3" of iron in the bottom of gap 3 + 1" of Al in the sides of gap 4 + 1" of Al in the sides of gap 4 (+ Aluminium floor)

The effects on the number of hits per channel and per event for the gaps 1, 3 and 4 (counting from 0) and for panels 1 and 4[1] are shown in figure 13. We concentrate on panels 1 and 4 because they are symmetric and panel 1 is totally unshielded, while panel 4 is nearly completely shielded. The thick shielding only effects bottom panels in the last two gaps, so focus attention on the bottom-middle and the bottom right panels of figure 13. From this figure we observe that 2" and 6" reduce the panel 4 hit rate to 58% and 33% of its pre-shielding value (respectively), confirming our expectation that more shielding is better.

So, to efficiently reduce particles of different types (mainly electrons, pions and protons) coming from the beam-pipe and hitting the MuID, 6" of iron seems to be the good solution.

Shielding simulations.

To confirm this and to determine what would be the best geometry, two shielding options were simulated and studied:

- A continuous shielding in the floor and the sides of gaps 1 to 4 with 6" of iron (labeled Peter Kroon's configuration C) .
- A continuous shielding in the floor and columns, to shield only the panels and not the absorbers of the MuID, on the sides of gaps 1 to 4 with 6" of iron (labeled Peter Kroon's configuration D).

For both of these configurations, a 60×60 cm^2 hole was left in the floor to allow room for the vacuum pump. A small hole exists also on the west wall convering gap 4 to have access to a shut-off valve. This is shown in figure 14 which is the PISA representation of the square-hole region for the configuration with the continuous shielding (Peter Kroon's configuration C). The large black and blue parallelepipeds represent the MuID panels. The blue and red cylinders correspond to the cover and the inner part of the DX magnet. The turquoise parallelepipeds display the iron shielding walls and the 2 pink parallelepipeds the holes for the vacuum valve and the shut off valve.

The occupancy per gap for each panel is shown in figure 15. In this figure the comparison is made with the simulation with only the aluminium floor (i.e. no added shielding). The numbers of hits in the MuID for the 4 shielded gaps (1, 2 ,3 and 4) and the 5 shielded panels (all panels except the upper small panel, panel 1) are reduced by 40 % with the column side shielding and by 49 % with the continuous shielding.

So it was decided to install the shielding with the continuous sides. This was done October the 10th.

[1]Panel 1 is the small upper panel and the panel 4 is the small lower panel.

5 Results with the iron shielding.

Occupancy

The occupancy per gap obtained with the iron shielding is presented in figure 16 and is compared to the simulations and to the configuration without shielding. We observe that the occupancy for the shielded panels (i.e. all gaps except gap 0 and all panels except panel 1) has been reduced by 5%, 23%, 63% and 58% for the gap 1, 2, 3 and 4 respectively and that simulations data are in good agreement.

Rejection factor.

The comparison of the rejection factors obtained for different triggers before and after the iron shielding was installed are listed in table 1, where are also reported the specifications of the triggers. The values of the rejection factor are calculated masking panel 1 (i.e., we do not consider data coming from this panel for the trigger) of each gap as this panel is not shielded.

Trigger name	Minimum angle	Centrality	Opening angle	RF before	RF after
DiMuon	12°	0-100 %	19°	6	44
DiMuonPeripheral	12°	40-100 %	19°	62	571
SingleMuon	12°	0-100 %		2	7
SingleMuonPeripheral	12°	40-100 %		12	56

Table 1: *Measured rejection factors obtained for the different dimuon and single muon triggers before the shielding (i.e. with no shielding) and after installing the iron shielding.*

From table 1 we see a considerable improvement of the rejection factor for the dimuon trigger: it is better by a factor of 7.3 for the minimum bias events and a factor of 9.2 for the peripheral events.

The rejection factors before shielding were low enough that they were essentially useless. In order to fit into our bandwidth budget, we would have needed to scale them down by roughly a factor 10. At this level of scaledown it would have been just about as good to simply collect minimum bias data.

References

[1] *https://www.phenix.bnl.gov:8080/phenix/WWW/p/draft/vince/anal_notes/muidlvl2/simulations.html*

[2] P. Deines-Jones *et al.*, *Phys. Rev.* **C 62** (2000) 014903.

[3] I. G. Bearden *et al.*, BRAHMS collaboration, *Phys. Lett.* **B 523** (2001) 227.

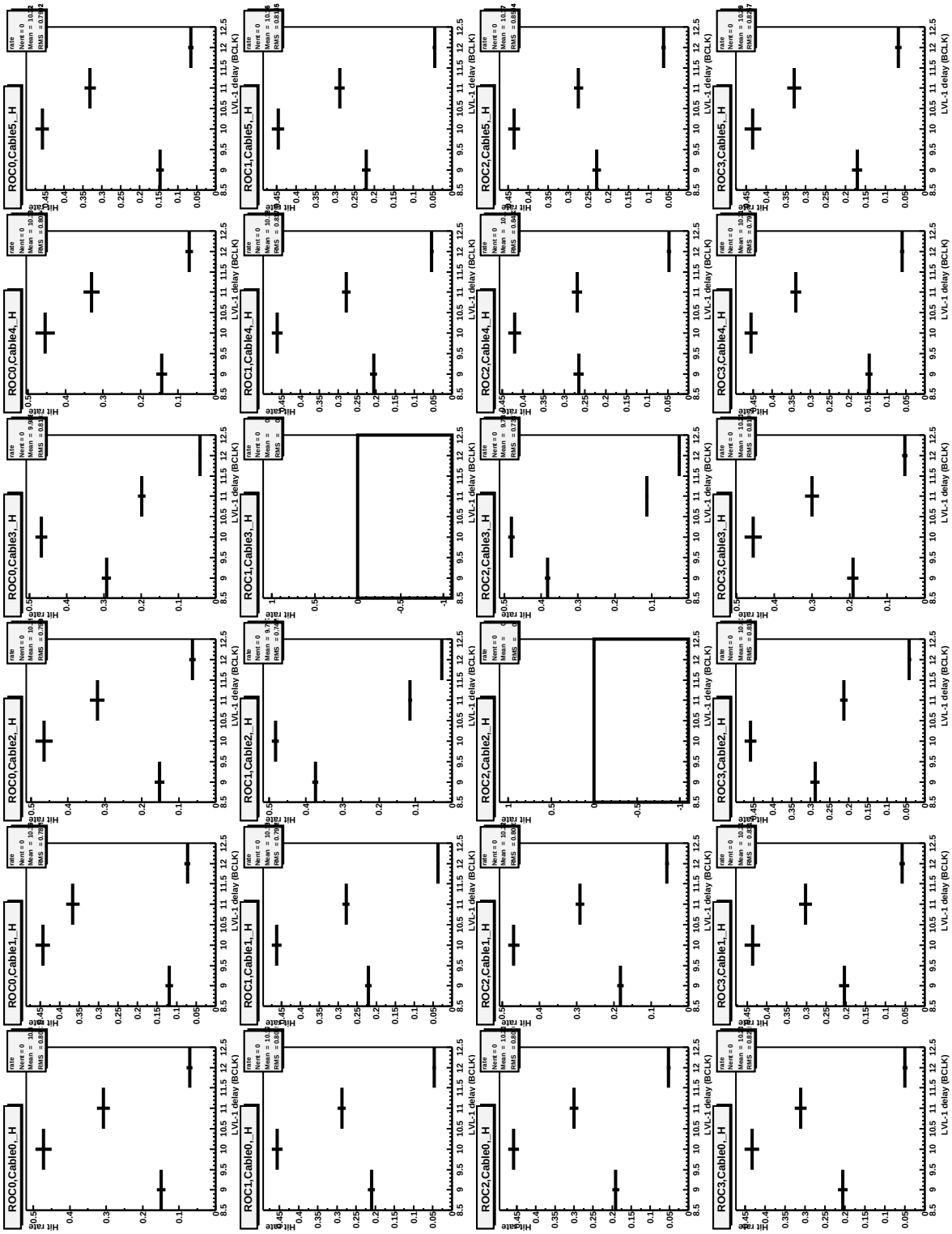

Figure 2: *Beam-Beam Local level 1 delay of the MuID cables corresponding to the horizontal tubes of gap 0 (in beam clock unit).*

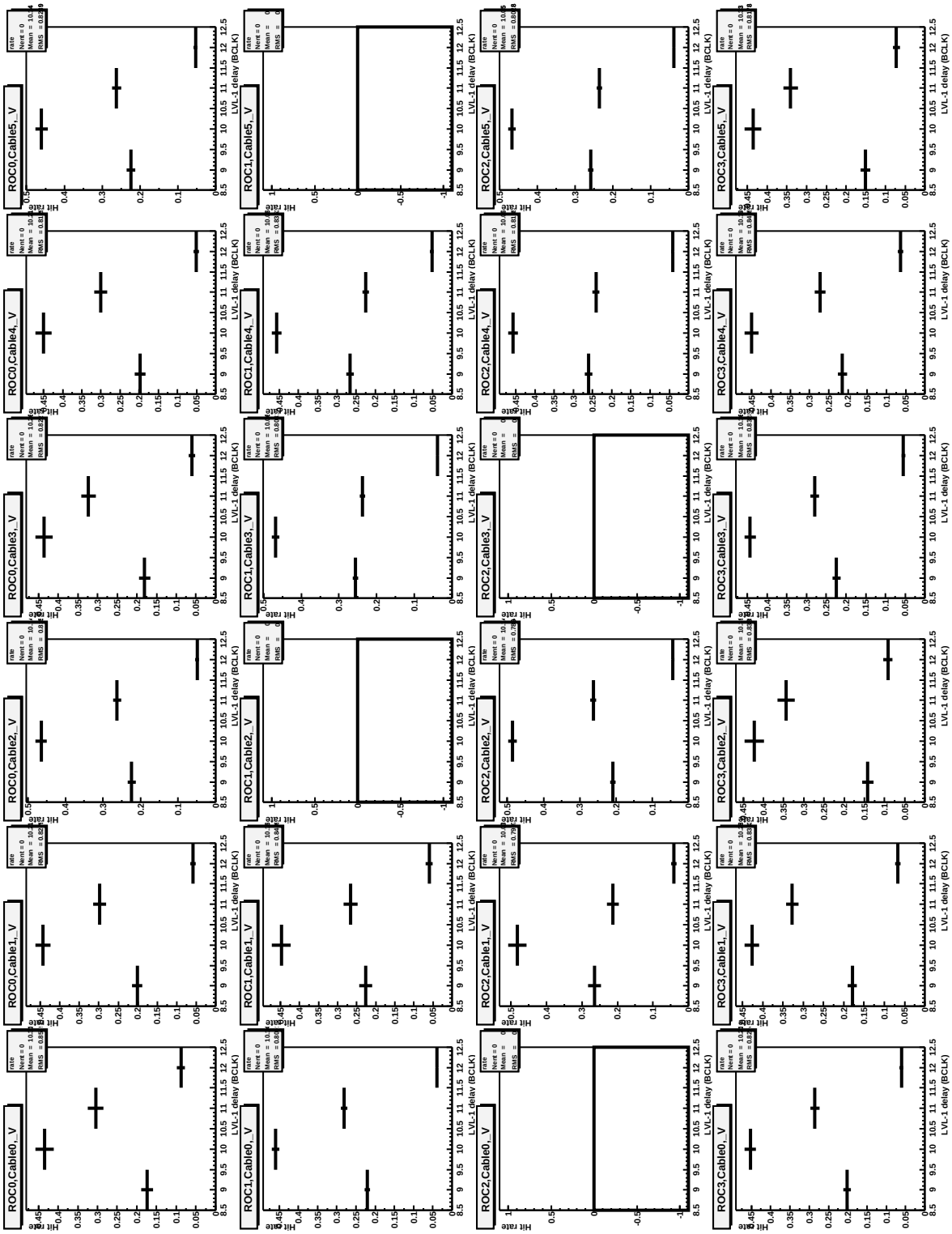

Figure 3: *Beam-Beam Local level 1 delay of the MuID cables corresponding to the vertical tubes of gap 0 (in beam clock unit).*

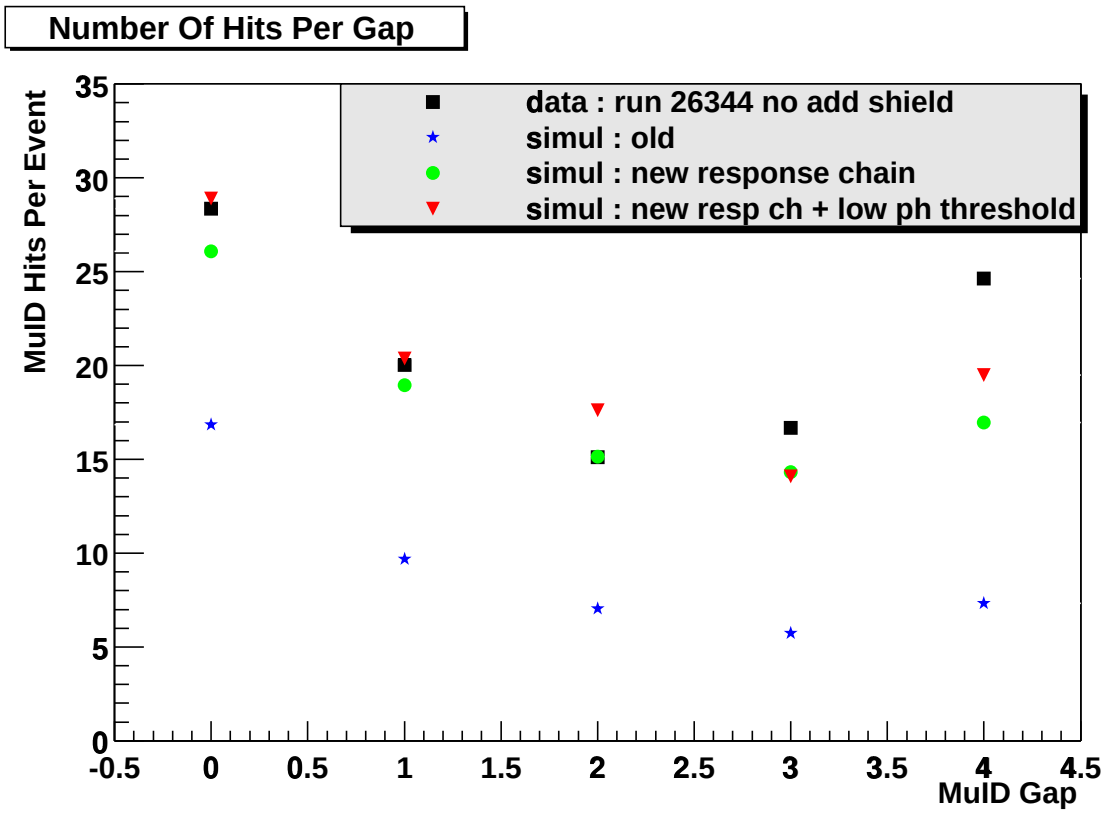

Figure 4: *Number of hits per gap and per event, for the configuration with no added shielding, obtained for the experimental data and different simulations (see the text for explanations). Note: the statistical error is smaller than the symbols.*

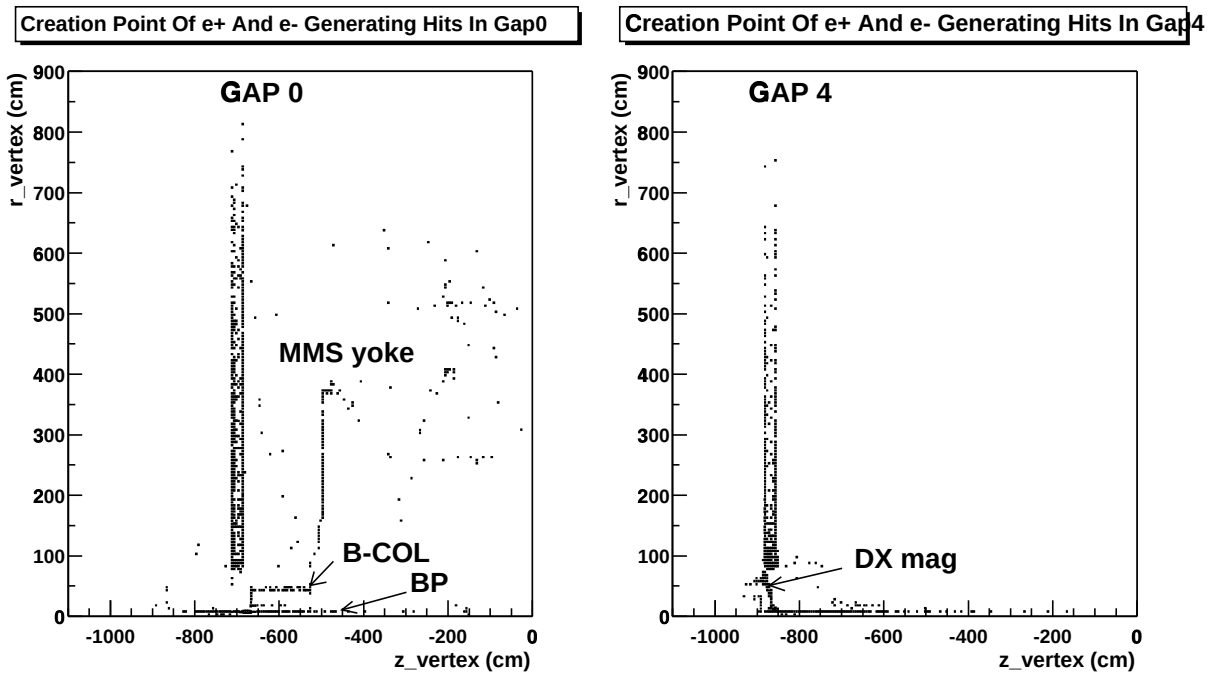

Figure 5: *Creation point of the positrons and electrons which have fired Iarocci tubes in gap 0 and gap 4. The words indicate the different elements of the experimental setup and of the collider: "MMS yoke" for the yoke of the south muon magnet, "BP" for beam-pipe, "B-COL" for beam collar, "DX mag" for DX magnet.*

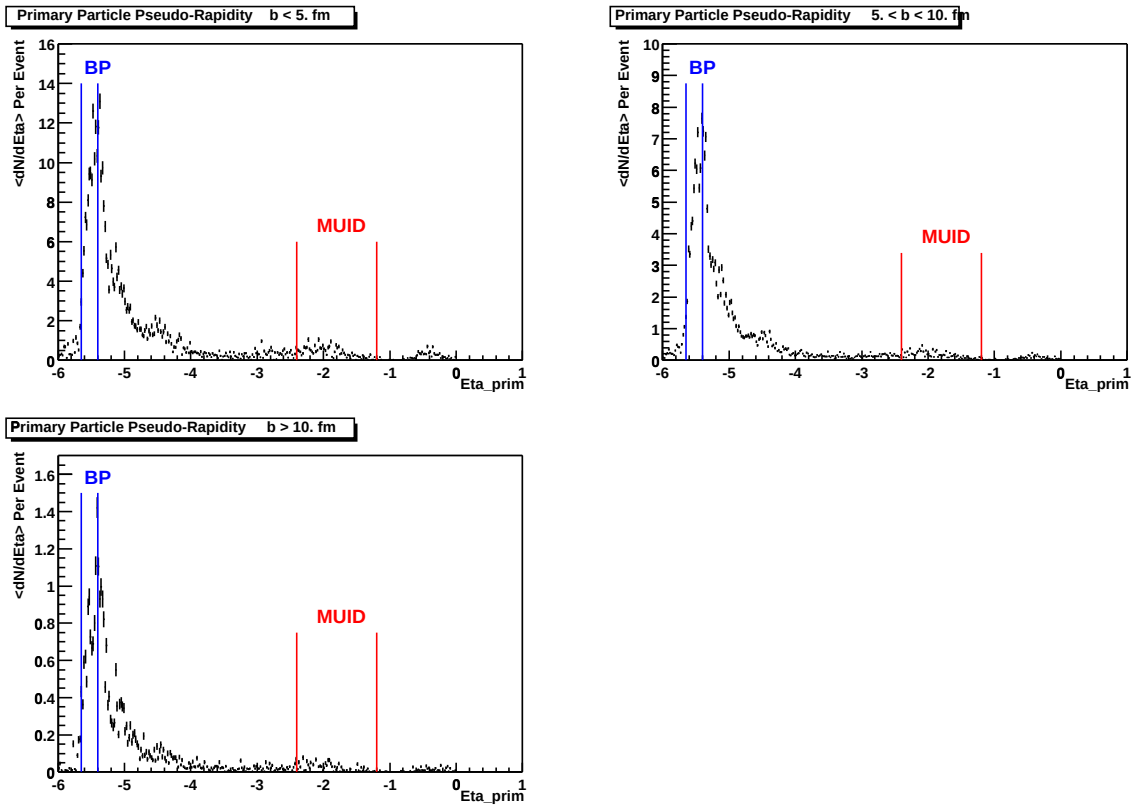

Figure 6: *Average pseudo-rapidity distribution per event (obtained after the improvement of the simulation) of the primary parents of particles which produce a hit in the MuID, for three impact parameter bins.*

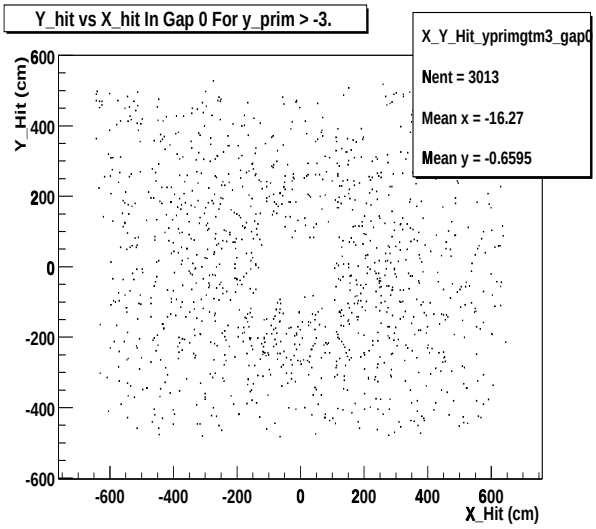

Figure 7: *X versus Y of the hits in gap 0 corresponding to primary particles with* $y_{prim} > -3$.

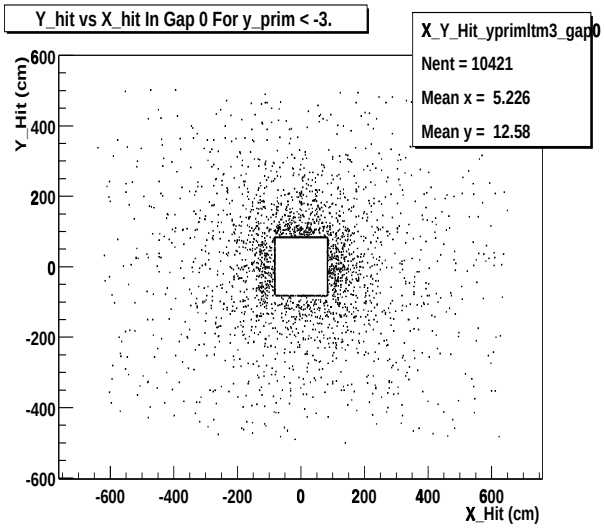

Figure 8: *X versus Y of the hits in gap 0 corresponding to primary particles with* $y_{prim} < -3$.

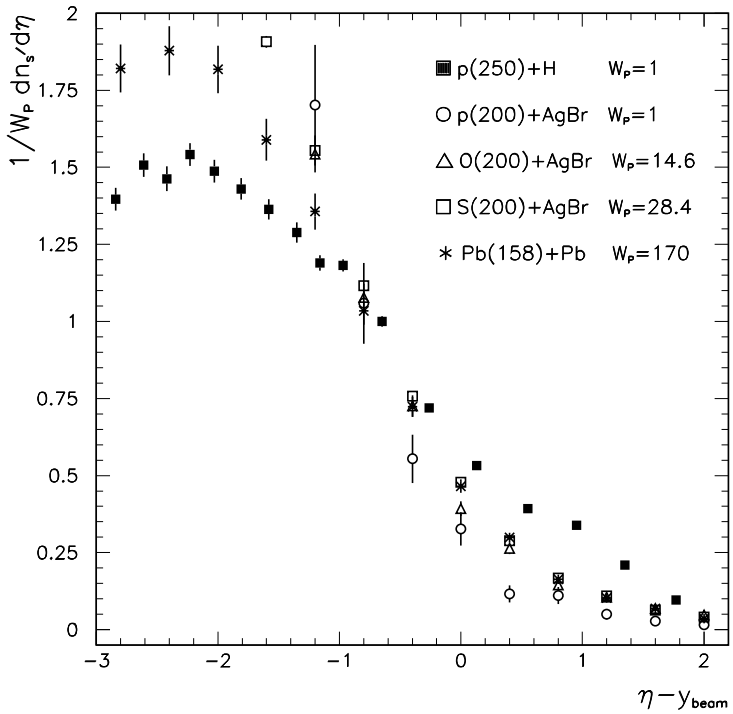

Figure 9: *Charged density divided by the number of projectile nucleons in the beam frame versus* $\eta' = \eta - y_{beam}$ *obtained at CERN/SPS for proton projectiles at 250 GeV/c and 200 GeV/c, for oxygen and sulfur projectiles at 200 GeV/c per nucleon and lead projectiles at 158 GeV/c per nucleon (from [2]).*

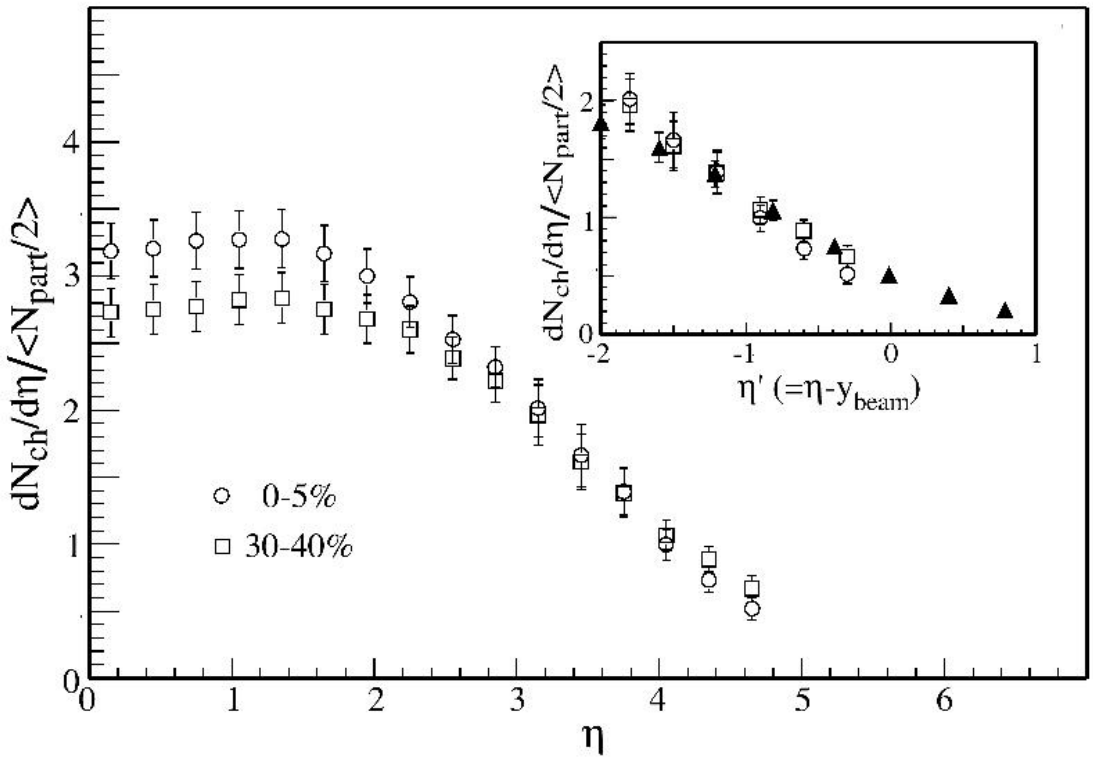

Fig. 3. Charged particle densities normalized to the number of participant pairs. Total (statistical + systematic) uncertainties are shown, not including the uncertainty in $< N_{part} >$ (see text). The insert compares the 0-5% central (open circles) and 30-40% central (open squares) Au+Au results to the 9.4% central Pb+Pb data (closed triangles) of ref. [4]. For this comparison of the "projectile" regions for the two reactions, the data are plotted in terms of the pseudorapidity shifted by the beam rapidity, as discussed in the text. For the insert, the particle densities are normalized to the number of projectile participants, which is equal to the number of participant pairs for a symmetric reaction.

Figure 10: *Charged density divided by $N_{part}/2$ versus the pseudo-rapidity obtained by BRAHMS experiment in Au-Au collisions at $\sqrt{s} = 130$ GeV [3]. Inserted: comparison of the charged density divided by $N_{part}/2$ versus $\eta' = \eta - y_{beam}$ in Au-Au collisions at $\sqrt{s} = 130$ GeV at RHIC and Pb-Pb collisions at 158 GeV/c per nucleon at CERN/SPS ($\sqrt{s} = 17$ GeV) [2].*

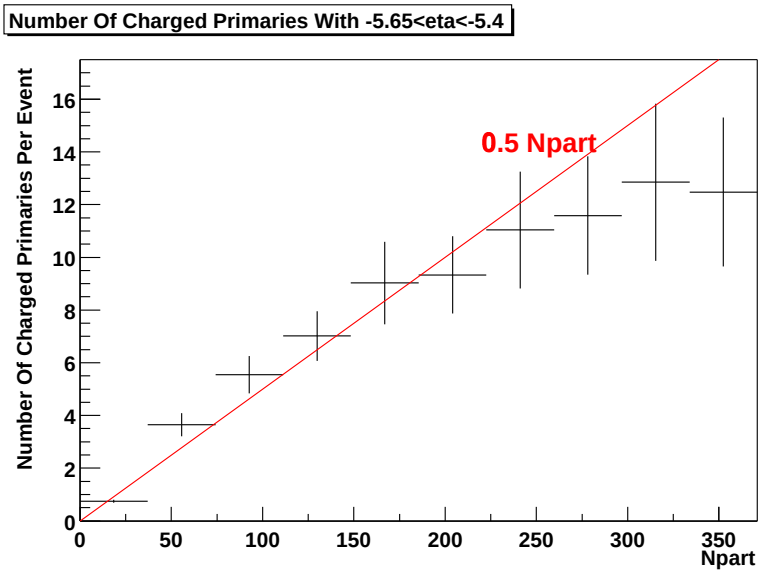

Figure 11: *Charged multiplicity versus N_{part} in Au-Au collisions at $\sqrt{s} = 200$ GeV for $\eta = [-5.65, -5.4]$ extracted from HIJING. The line represents the charged multiplicity dependance with N_{part} deduced from the hypothesis of limiting fragmentation (see the text for explanation).*

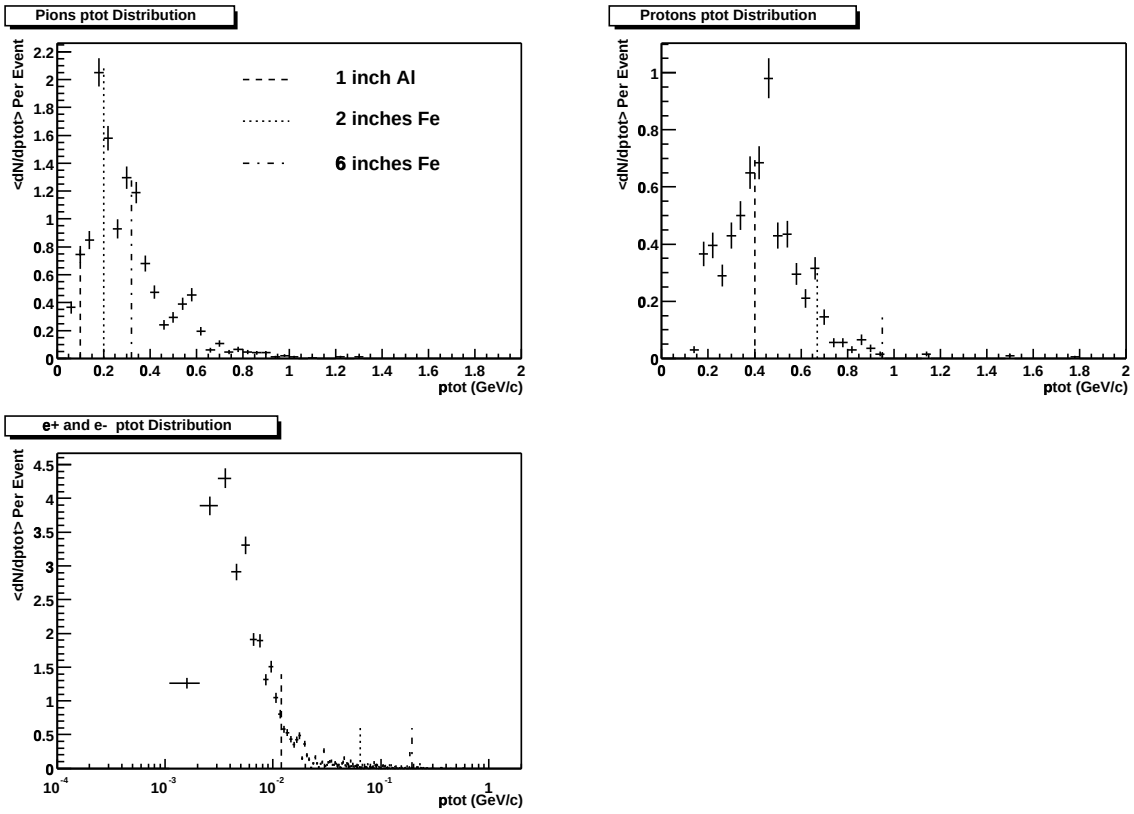

Figure 12: *Total momentum distribution of the pions, protons, positrons and electrons created in the beam-pipe region or the DX magnet region, when they enter the sensitive volume of the MuID.*

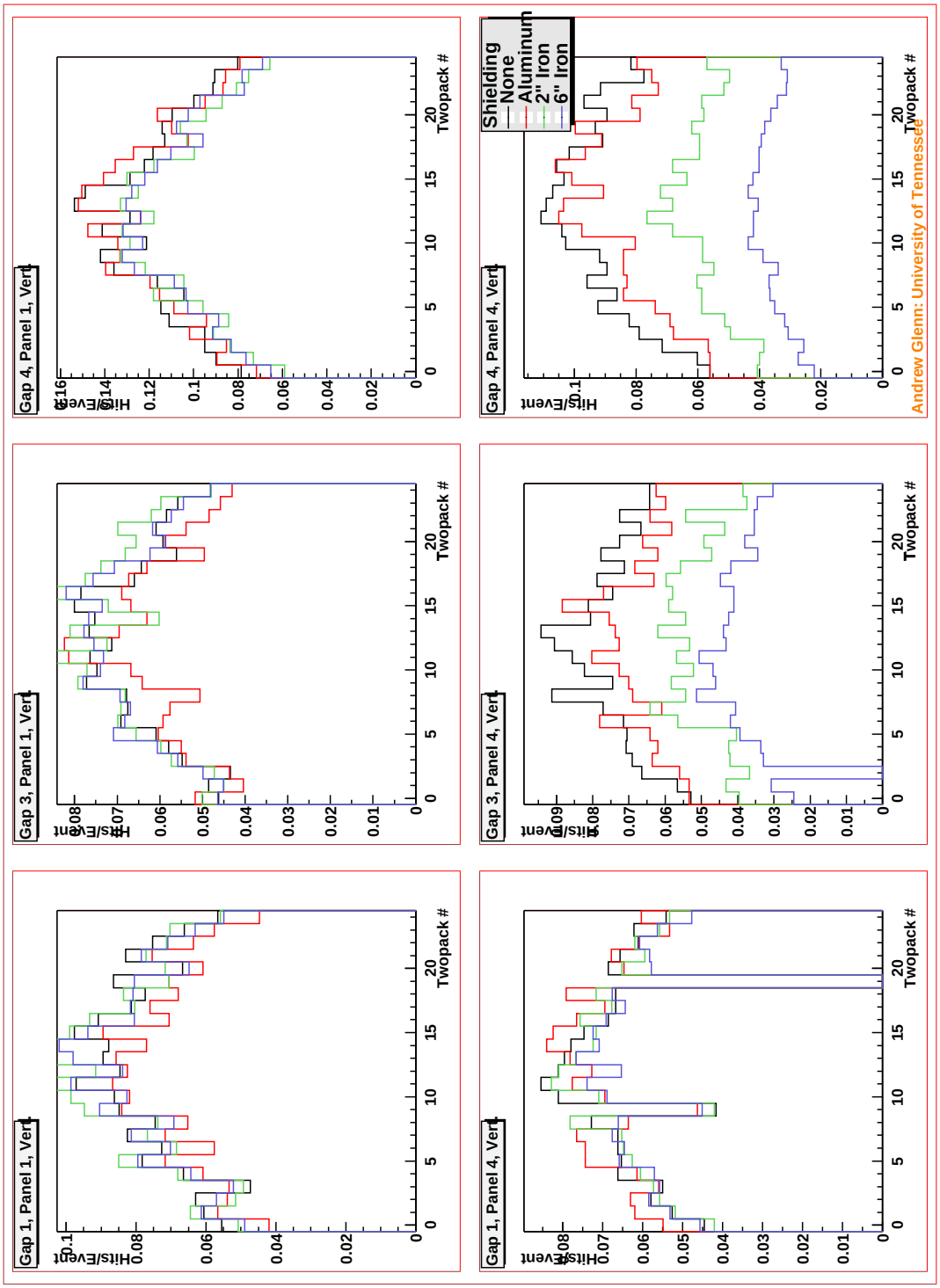

Figure 13: *Number of hits per twopack and per event obtained for different shielding configurations.*

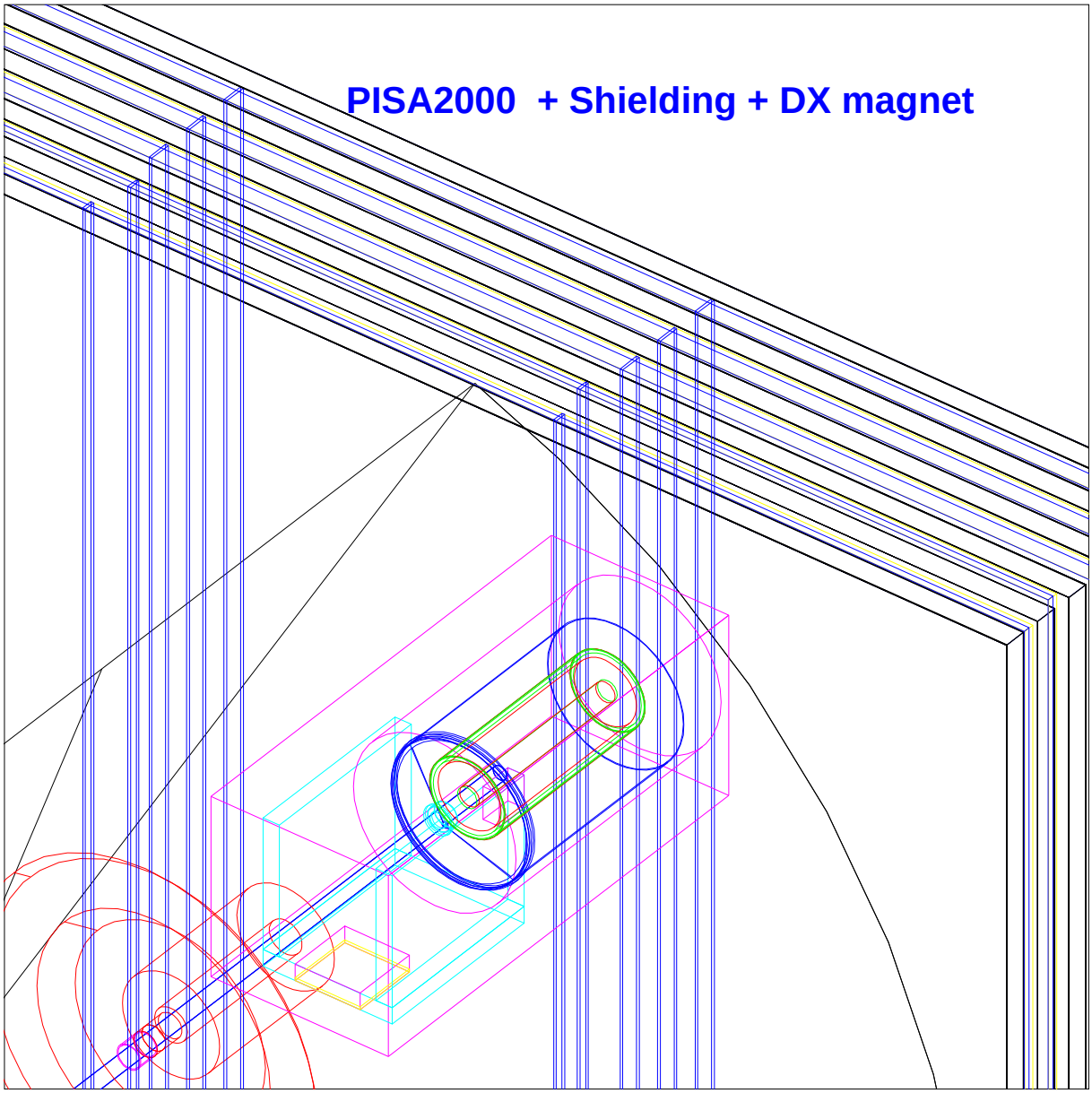

Figure 14: *PISA drawing of the MuID square-hole for the configuration with the continuous walls of iron shielding.*

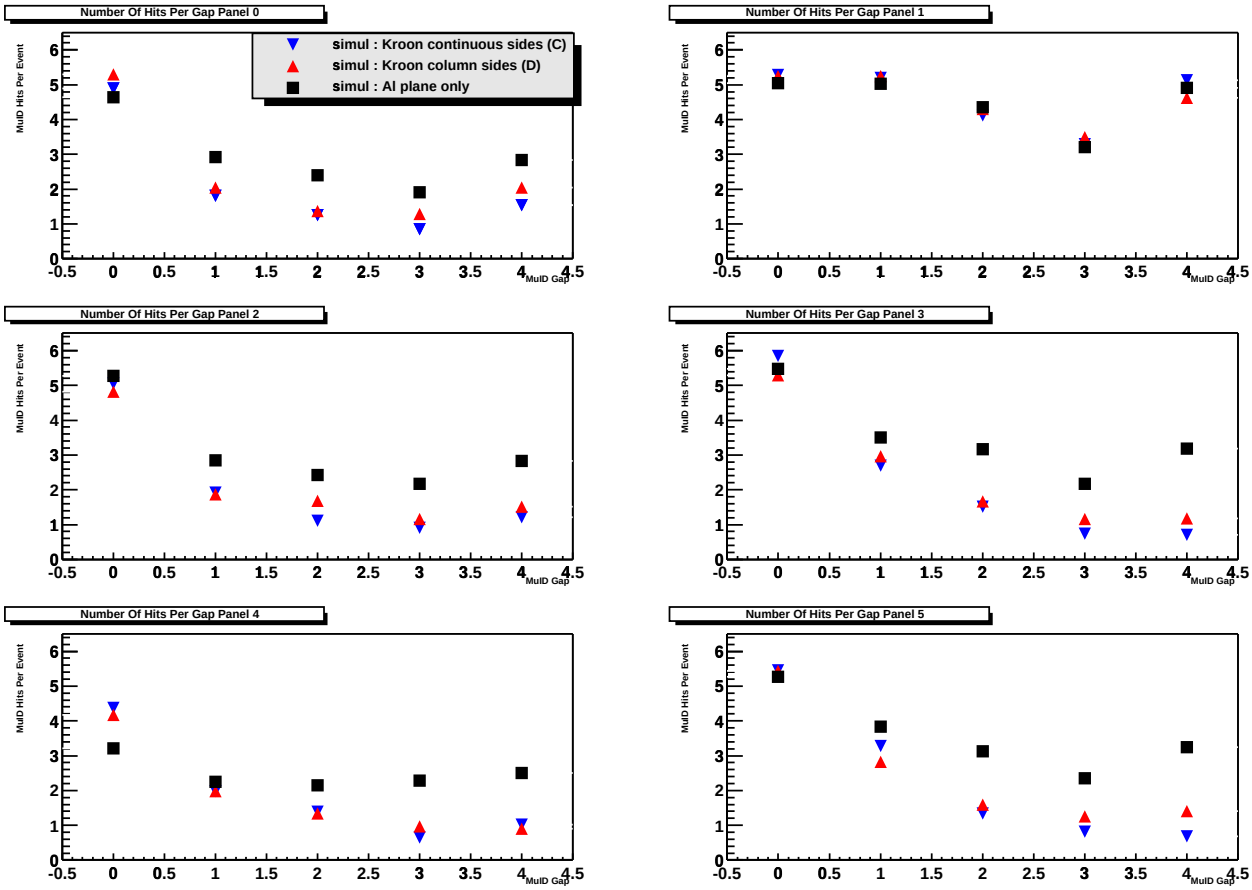

Figure 15: *Simulated occupancy per gap and per event for each panel obtained for the two proposed configurations of iron shielding, compared to the occupancy without added shielding.*

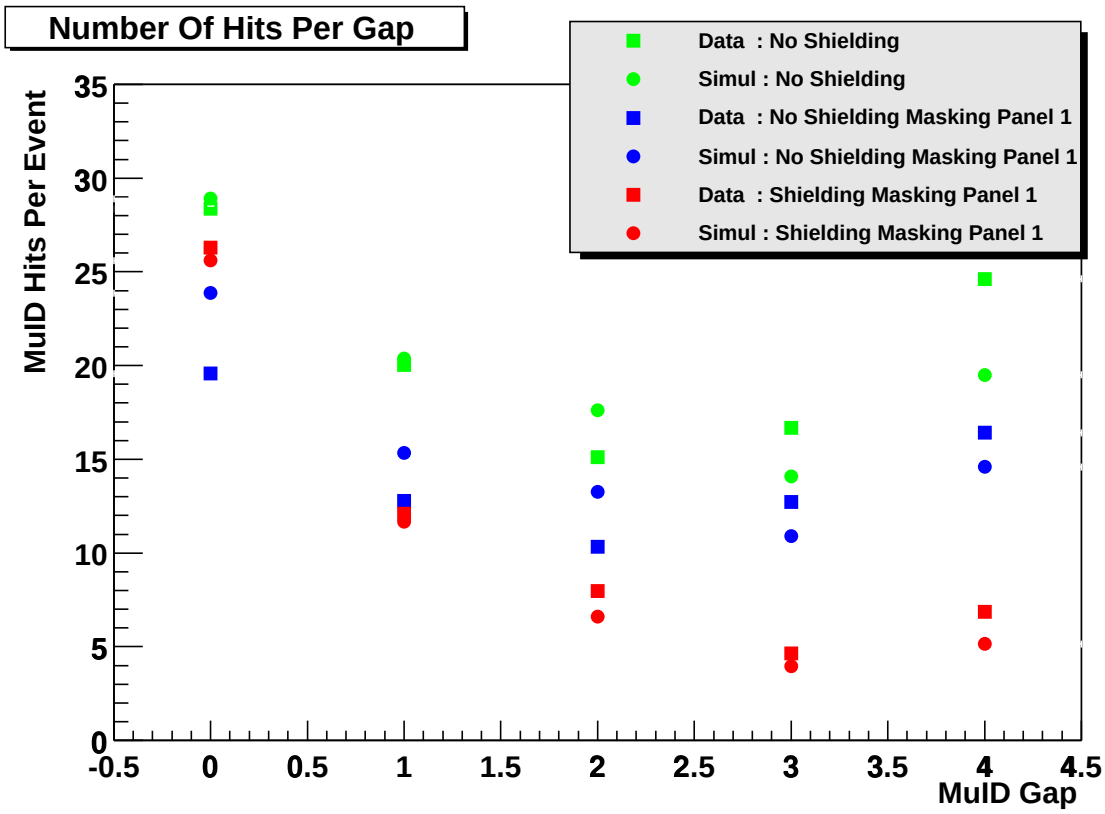

Figure 16: *Average occupancy per gap of the real data and simulations for the configuration with no added shielding and with iron shielding. Note: the statistical error is smaller than the symbols.*